Electronic structure and optical properties of ZnX (X=O, S, Se, Te): A density functional study

S. Zh. Karazhanov,[1,2] P. Ravindran,[1] A. Kjekshus,[1] H. Fjellvåg,[1] and B. G. Svensson[3]
[1]*Centre for Material Science and Nanotechnology, Department of Chemistry, University of Oslo, P.O. Box 1033 Blindern, N-0315 Oslo, Norway*
[2]*Physical-Technical Institute, 2B Mavlyanov Street, Tashkent 700084, Uzbekistan*
[3]*Department of Physics, University of Oslo, P.O. Box 1048 Blindern, N-0316 Oslo, Norway*
(Received 5 July 2006; revised manuscript received 15 November 2006; published 6 April 2007)

Electronic band structure and optical properties of zinc monochalcogenides with zinc-blende- and wurtzite-type structures were studied using the *ab initio* density functional method within the local-density approximation (LDA), generalized-gradient approximation, and LDA+U approaches. Calculations of the optical spectra have been performed for the energy range 0–20 eV, with and without including spin-orbit coupling. Reflectivity, absorption and extinction coefficients, and refractive index have been computed from the imaginary part of the dielectric function using the Kramers-Kronig transformations. A rigid shift of the calculated optical spectra is found to provide a good first approximation to reproduce experimental observations for almost all the zinc monochalcogenide phases considered. By inspection of the calculated and experimentally determined band-gap values for the zinc monochalcogenide series, the band gap of ZnO with zinc-blende structure has been estimated.

DOI: 10.1103/PhysRevB.75.155104 PACS number(s): 71.15.−m, 71.22.+i

I. INTRODUCTION

The zinc monochalcogenides (ZnX; X=O, S, Se, and Te) are the prototype II-VI semiconductors. These compounds are reported to crystallize in the zinc-blende-(z) and wurtzite (w)-type structures. The ZnX-z phases are optically isotropic, while the ZnX-w phases are anisotropic with c as the polar axis. ZnX phases are a primary candidate for optical device technology such as visual displays, high-density optical memories, transparent conductors, solid-state laser devices, photodetectors, solar cells, etc. So, knowledge about optical properties of these materials is especially important in the design and analysis of ZnX-based optoelectronic devices.

Optical parameters for some of the ZnX phases have widely been studied experimentally in the past. Detailed information on this subject is available for ZnO-w,[1–9] ZnS-w,[9] ZnS-z,[9–11] ZnSe-z,[9,10] and ZnTe-z,[9,10,12,13] and see the systematized survey in Ref. 14. However, there are no experimental data on optical properties of ZnSe-w, ZnTe-w, and ZnO-z. Furthermore, there is a lack of consistency between some of the experimental values for the optical spectra. This is demonstrated in Fig. 1, which displays reflectivity spectra for ZnO-w measured at T=300 K by three different groups. Dielectric-response functions were calculated using the Kramers-Kronig relation. As is seen in Fig. 1, intensity of the imaginary part of the dielectric function (ϵ_2) and reflectivity (R) corresponding to the fundamental absorption edge of ZnO-w are higher[8] than those at the energy range 10–15 eV, while in Ref. 14 it is vice versa. The optical spectra in Fig. 1 measured using the linearly polarized incident light for electric field (E) parallel ($\parallel$) and perpendicular ($\perp$) to the c axes are somehow close to those of Ref. 7 using nonpolarized incident light.

Using the experimental reflectivity data, a full set of optical spectra for ZnO has been calculated[15] for the wide energy range 0–26 eV. Density functional theory[16] (DFT) in the local-density approximation[17] (LDA) has also been used to calculate optical spectra for ZnO-w (Ref. 18) and ZnS-w (Ref. 18) by linear combination of atomic orbitals and for ZnS-z[19] and ZnSe-z[19] by self-consistent linear combination of Gaussian orbitals. The optical spectra of ZnO (including excitons) has been investigated[20] by solving the Bethe-Salpeter equation. Band-structure studies have been performed by linearized-augmented plane-wave method plus local orbitals (LAPW+LO) within the generalized gradient and LDA with the multiorbital mean-field Hubbard potential (LDA+U) approximations. The latter approximation is found to correct not only the energy location of the Zn 3d electrons and associated band parameters (see also Refs. 21 and 22) but also to improve the optical response. Despite the shortcoming of DFT in relation to underestimation of band gaps, the locations of the major peaks in the calculated energy dependence of the optical spectra are found to be in good agreement with experimental data.

It should be noted that the error in calculation of the band gap by DFT within LDA and generalized-gradient approximation (GGA) is more severe in semiconductors with strong Coulomb correlation effects than in other solids.[21–25] This is due to the mean-field character of the Kohn-Sham equations and the poor description of the strong Coulomb correlation and exchange interaction between electrons in narrow d bands (viz., the potential U). Not only the band gap (E_g) but also the crystal-field (CF) and spin-orbit (SO) splitting energies (Δ_{CF} and Δ_{SO}), the order of states at the top of the valence band (VB), the location of the Zn 3d band and its width, and the band dispersion are found[21,22,26,27] to be incorrect for ZnO-w by the *ab initio* full potential (FP) and atomic-sphere-approximation (ASA) linear muffin-tin orbital (LMTO) methods within the pure LDA (Refs. 26 and 27) and by the projector-augmented wave (PAW) method within LDA and GGA.[21,22] These findings were ascribed[21,22] to strong Coulomb correlation effects. DFT calculations within LDA plus self-interaction correction (LDA+SIC) and LDA+U are found[21,22,26] to rectify the errors related to Δ_{CF} and

 ©2007 The American Physical Society

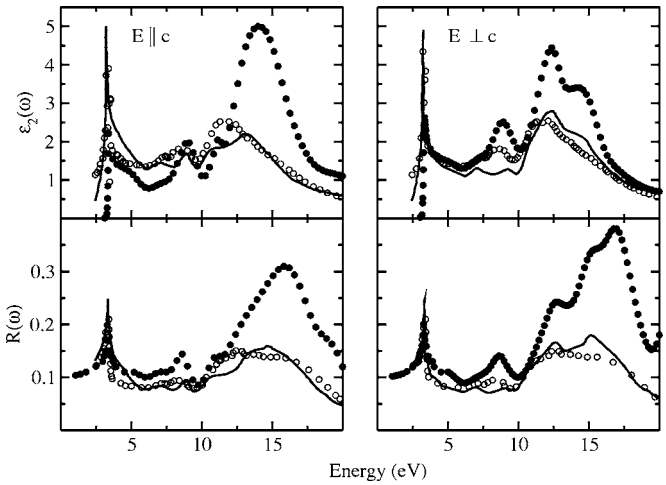

FIG. 1. Reflectivity spectra $R(\omega)$ for ZnO-*w* determined experimentally at 300 K in Refs. 9 and 14 (solid circles), Ref. 8 (open circles), and Ref. 7 (solid lines), along with the imaginary part of the dielectric-response function $[\epsilon_2(\omega)]$ calculated using the Kramers-Kronig relation. The results of Ref. 7 (open circles) are used for both $E\|c$ and $E\perp c$, because no polarized incident light was used in the experiments.

Δ_{SO}, order of states at the top VB, and width and location of the Zn 3*d* band, as well as effective masses. In other semiconductors, in which the Coulomb correlation is not sufficiently strong, the Δ_{CF} and Δ_{SO} values derived from DFT calculations within LDA are found to be quite accurate. This was demonstrated for diamondlike group IV, *z*-type group III-V, II-VI, and I-VII semiconductors,[28] *w*-type AlN, GaN, and InN,[29] using the LAPW and VASP-PAW, the *w*-type CdS and CdSe,[27] *z*-type ZnSe, CdTe, and HgTe,[30] using the *ab initio* LMTO-ASA, and *z*- and *w*-type ZnSe and ZnTe (Refs. 21 and 22) as well as *z*-type CdTe,[31] using the VASP-PAW and FP LMTO methods. Although the SO splitting at the top of VB is known to play an important role in electronic structure and chemical bonding of semiconductors,[21,22,26,28–30,32,33] there is no systematic study of the role of the SO coupling in optical properties of these materials.

Several attempts have been undertaken to resolve the DFT eigenvalue problem. One such approach is the utilization of the GW approximation ("G" stands for one-particle Green's function as derived from many-body perturbation theory and "W" for Coulomb screened interactions). Although GW removes most of the problems of LDA with regard to excited-state properties, it fails to describe the semiconductors with strong Coulomb correlation effects. For example, two studies of the band gap of ZnO calculated using the GW correction underestimated E_g by 1.2 eV (Ref. 34) and overestimated it by 0.84 eV.[35] Calculations for Zn, Cd, and Hg monochalcogenides by the GW approach showed[36] that the band-gap underestimation is in the range 0.3–0.6 eV. Combination of exact-exchange (EXX) DFT calculations and the optimized-effective GW potential approach is found[37] to improve the agreement with the experimental band gaps and Zn 3*d* energy levels. Band gaps calculated within the EXX treatment are found to be in good agreement with experiment for the *s-p* semiconductors.[38,39] Excellent agreement with experimental data was obtained[39] also for locations of energy levels of the *d* bands of a number of semiconductors and insulators such as Ge, GaAs, CdS, Si, ZnS, C, BN, Ne, Ar, Kr, and Xe.

Another means to correct the DFT eigenvalue error is to use the screened-exchange LDA.[40] Compared to LDA and GW, this approximation is found to be computationally much less demanding, permitting self-consistent determination of the ground-state properties and giving more correct band gaps and optical properties. Other considered approaches for *ab initio* computations of optical properties involve electron-hole interaction,[41] partial inclusion of dynamical vertex corrections that neglect excitons,[42] and empirical energy-dependent self-energy correction according to the Kohn-Sham local-density theory of excitation.[19] However, the simplest method is to apply the scissor operator,[43] which displaces the LDA eigenvalues for the unoccupied states by a rigid energy shift. Using the latter method, excellent agreement with experiments has been demonstrated for lead monochalcogenides[44] and ferroelectric $NaNO_2$.[45] However, the question as to whether the rigid energy shift is generally applicable to semiconductors with strong Coulomb correlation effects is open.

In this work, electronic structure and optical properties of the Zn*X*-*w* and -*z* phases have been studied in the energy range from 0 to 20 eV based on first-principles band-structure calculations derived from DFT within the LDA, GGA, and LDA+*U*.

II. COMPUTATIONAL DETAILS

Experimentally determined lattice parameters have been used in the present *ab initio* calculations (Table I). The ideal positional parameter *u* for Zn*X*-*w* is calculated on the assumption of equal nearest-neighbor bond lengths:[27]

$$u = \frac{1}{3}\left(\frac{a}{c}\right)^2 + \frac{1}{4}. \quad (1)$$

The values of *u* for the ideal case agree well with the experimental values u^* (see Table I). Self-consistent calculations were performed using a $10\times10\times10$ mesh according to the Monkhorst-Pack scheme for the Zn*X*-*z* phases and the Γ-centered grid for the Zn*X*-*w* phases.

A. Calculations by VASP package

Optical spectra have been studied based on the band-structure data obtained from the VASP-PAW package,[55] which solves the Kohn-Sham eigenvalues in the framework of the DFT (Ref. 16) within LDA,[17] GGA,[56] and the simplified rotationally invariant LDA+*U*.[23,24] The exchange and correlation energies per electron have been described by the Perdew-Zunger parametrization[57] of the quantum Monte Carlo results of Ceperley and Alder.[58] The interaction between electrons and atomic cores is described by means of non-norm-conserving pseudopotentials implemented in the VASP package.[55] The pseudopotentials are generated in accordance with the PAW (Refs. 59 and 60) method. The use of the PAW pseudopotentials addresses the problem of inad-

TABLE I. Theoretically and experimentally (in brackets) determined unit-cell dimensions a and c, volumes V, ideal u [calculated by Eq. (1)], and experimental u^*, as well as values of the parameters U and J from Refs. 21 and 22, were used in the present calculations. For w-type structure, $a=b$. For the z-type structure, $a=b=c$ and all atoms are in fixed positions.

Phase	a (Å)	c (Å)	V (Å^3)	u^*	u	U (eV)	J (eV)
ZnO-w[a]	3.244(3.250)	5.027(5.207)	45.82(47.62)	0.383	0.380	9	1
ZnS-w[b,c]	3.854(3.811)	6.305(6.234)	81.11(78.41)	0.375	0.375	6	1
ZnSe-w[a,d]	4.043(3.996)	6.703(6.626)	94.88(91.63)	0.375	0.371	8	1
ZnTe-w[e,f]	4.366(4.320)	7.176(7.100)	118.47(114.75)	0.375	0.373	7	1
ZnO-z[g]	4.633(4.620)		99.45(98.61)			8	1
ZnS-z[h,i]	5.451(5.409)		161.99(158.25)			9	1
ZnSe-z[a]	5.743(5.662)		189.45(181.51)			8	1
ZnTe-z[i,j]	6.187(6.101)		236.79(227.09)			8	1

[a]Reference 46.
[b]Reference 18.
[c]Reference 47.
[d]Reference 48.
[e]Reference 49.
[f]Reference 50.
[g]Reference 51.
[h]Reference 52.
[i]Reference 53.
[j]Reference 54.

equate description of the wave functions in the core region (common to other pseudopotential approaches[61]), and its application allows us to construct orthonormalized all-electron-like wave functions for Zn $3d$ and $4s$ and s and p valence electrons of the X atoms under consideration. LDA and GGA pseudopotentials have been used, and the completely filled semicore Zn $3d$ shell has been considered as valence states.

It is well known that DFT calculations within LDA and GGA locate the Zn $3d$ band inappropriately close to the topmost VB, hybridizing the O p band, falsifying the band dispersion, and reducing the band gap. Nowadays, the problem is known to be solved by using the LDA+SIC and LDA $+U$.[21,22,26,62–64] For the DFT calculations within LDA$+U$, explicit values of the parameters U and J are required as input. In previous papers,[21,22] we have estimated the values of the U and J parameters within the constrained DFT theory[65] and in a semiempirical way by performing the calculations for different values of U and forcing it to match the experimentally established[66] location of the Zn $3d$ bands. Based on the results,[21,22] the values of the parameters U and J listed in Table I are chosen to study the optical spectra.

B. Calculations by MINDLAB package

For investigation of the role of the SO coupling in electronic structure and optical properties of ZnX, DFT calculations have been performed using the MINDLAB package,[67] which uses the full potential linear muffin-tin orbital (FP LMTO) method. For the core charge density, the frozen-core approximation is used. The calculations are based on LDA with the exchange-correlation potential parametrized according to Gunnarsson-Lundquist[68] and Vosko-Wilk-Nussair.[69] The base geometry in this computational method consists of a muffin-tin part and an interstitial part. The basis set is comprised of linear muffin-tin orbitals. Inside the muffin-tin spheres, the basis functions, charge density, and potential are expanded in symmetry-adapted spherical harmonic functions together with a radial function and a Fourier series in the interstitial.

C. Calculation of optical properties

From the DFT calculations, the imaginary part of the dielectric function $\epsilon_2(\omega)$ has been derived by summing transitions from occupied to unoccupied states for energies much larger than those of the phonons:

$$\epsilon_2^{ij}(\omega) = \frac{Ve^2}{2\pi\hbar m^2\omega^2}\int d^3\mathbf{k}\sum_{nn'}\langle \mathbf{kn}|p_i|\mathbf{kn}'\rangle \times\langle \mathbf{kn}'|p_j|\mathbf{kn}\rangle f_{\mathbf{kn}}(1-f_{\mathbf{kn}'})\delta(\epsilon_{\mathbf{kn}'}-\epsilon_{\mathbf{kn}}-\hbar\omega). \quad (2)$$

Here, $(p_x,p_y,p_z)=\mathbf{p}$ is the momentum operator, $f_{\mathbf{kn}}$ the Fermi distribution, and $|\mathbf{kn}\rangle$ the crystal wave function corresponding to the energy $\epsilon_{\mathbf{kn}}$ with momentum $\mathbf{k}$. Since the ZnX-w phases are optically anisotropic, components of the dielectric function corresponding to the electric field parallel ($E\|c$) and perpendicular ($E\perp c$) to the crystallographic c axis have been considered. The ZnX-z phases are isotropic; consequently, only one component of the dielectric function has to be analyzed.

The real part of the dielectric function $\epsilon_1(\omega)$ is calculated using the Kramer-Kronig transformation. The knowledge of

both the real and imaginary parts of the dielectric tensor allows one to calculate other important optical spectra. In this paper, we present and analyze the reflectivity $R(\omega)$, the absorption coefficient $\alpha(\omega)$, the refractive index $n(\omega)$, and the extinction coefficient $k(\omega)$:

$$R(\omega) = \left| \frac{\sqrt{\epsilon(\omega)} - 1}{\sqrt{\epsilon(\omega)} + 1} \right|^2, \tag{3}$$

$$\alpha(\omega) = \omega \sqrt{2\sqrt{\epsilon_1^2(\omega) + \epsilon_2^2(\omega)} - 2\epsilon_1(\omega)}, \tag{4}$$

$$n(\omega) = \sqrt{\frac{\sqrt{\epsilon_1^2(\omega) + \epsilon_2^2(\omega)} + \epsilon_1(\omega)}{2}}, \tag{5}$$

$$k(\omega) = \sqrt{\frac{\sqrt{\epsilon_1^2(\omega) + \epsilon_2^2(\omega)} - \epsilon_1(\omega)}{2}}. \tag{6}$$

Here, $\epsilon(\omega) = \epsilon_1(\omega) + i\epsilon_2(\omega)$ is the complex dielectric function. The calculated optical spectra yield unbroadened functions and, consequently, have more structure than the experimental ones.[44,45,70,71] To facilitate a comparison with the experimental findings, the calculated imaginary part of the dielectric function has been broadened. The exact form of the broadening function is unknown. However, analysis of the available experimentally measured optical spectra of Zn*X* shows that the broadening usually increases with increasing excitation energy. Also, the instrumental resolution smears out many fine features. These features have been modeled using the lifetime broadening technique by convoluting the imaginary part of the dielectric function with a Lorentzian with a full width at half maximum of $0.002(\hbar\omega)^2$ eV, increasing quadratically with the photon energy. The experimental resolution was simulated by broadening the final spectra with a Gaussian, where the full width at half maximum is equal to 0.08 eV.

III. RESULTS AND DISCUSSION

A. Band structure

The optical spectra are related to band dispersion and probabilities of interband optical transitions. So, it is of interest to analyze the electronic structure in detail. Band dispersions for Zn*X*-*w* and Zn*X*-*z* calculated by DFT within LDA and LDA+*U* are presented in Fig. 2. The general features of the band dispersions are in agreement with previous studies (see, e.g., Refs. 26, 62, and 72). It is seen from Fig. 2 that the conduction-band (CB) minima for Zn*X*-*w* and Zn*X*-*z* are much more dispersive than the VB maximum, which shows that the holes are much heavier than the CB electrons in agreement with experimental data[73,74] for the effective masses and calculated with FP LMTO and (Ref. 26) linear combination of atomic orbitals,[18] as well as with our findings.[21,21] Consequently, mobility of electrons is higher than that of holes. Furthermore, these features indicate that *p* electrons of *X* (that form the topmost VB states) are tightly bound to their atoms and make the VB holes less mobile.

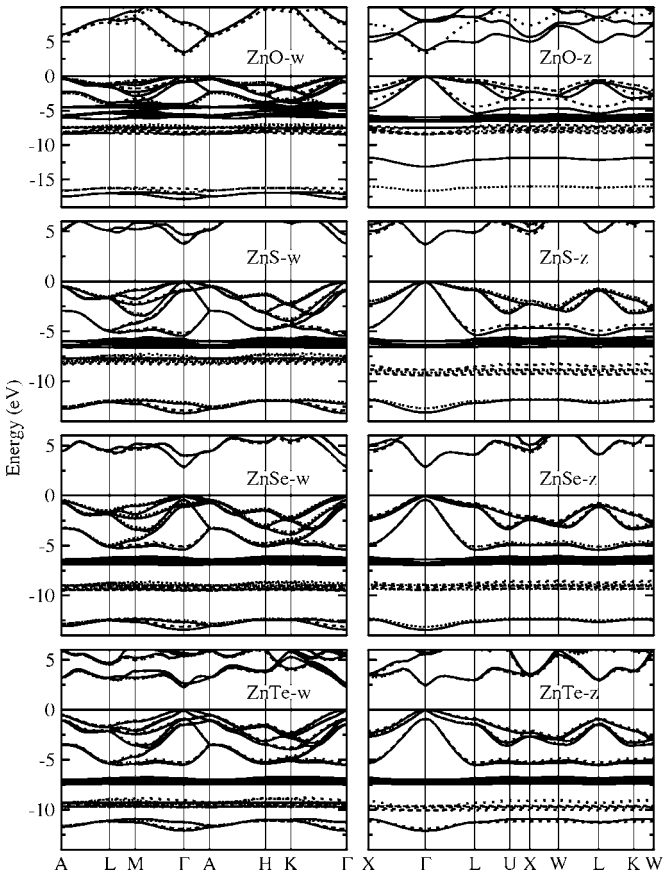

FIG. 2. Band dispersion for ZnO-*w*, ZnS-*w*, ZnSe-*w*, ZnTe-*w*, ZnO-*z*, ZnS-*z*, ZnSe-*z*, and ZnTe-*z* calculated according to LDA (solid lines) and LDA+*U* (dotted lines). The Fermi level is set to zero energy.

Hence, the contribution of the holes to the conductivity is expected to be smaller than that of CB electrons even though the concentration of the latter is smaller than that of the former. These features emphasize the predominant ionic nature of the chemical bonding. Another interesting feature of the band structures is that the VB maximum becomes more dispersive with increasing atomic number of *X* from O to Te.

As noted in our previous contributions,[21,22] the band gaps of Zn*X* calculated by DFT within LDA, GGA, and LDA+*U* are underestimated and the question as to whether it is possible to shift the CB states rigidly was kept open. As found from the optical spectra discussed on the following sections, rigid shifts of the CB states up to the experimentally determined locations can provide a good first approximation for the stipulation of the band gap. So, for the band dispersions in Fig. 2, we have made use of this simple way for correcting the band gaps calculated by DFT. The only problem in this respect was the lack of an experimental band-gap value for ZnO-*z*. To solve this problem, the experimental and calculated (by DFT within LDA) band gaps (E_g) of the Zn*X* series were plotted as a function of the atomic number of *X*. As seen from Fig. 3, E_g for the Zn*X*-*w* phases are very close to the corresponding values for the Zn*X*-*z* phases and the shape of the experimental and calculated functional dependencies is in conformity. On this basis, the

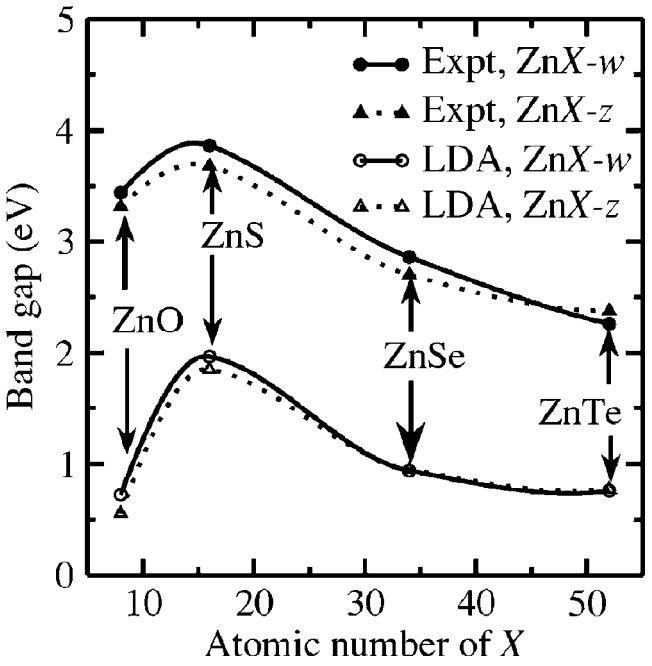

FIG. 3. Band gaps for Zn X-w (circles) and Zn X-z (triangles) phases determined experimentally (filled symbols, from Refs. 21 and 22) and calculated (open symbols) by DFT within LDA as a function of the atomic number of the X component of ZnX.

band gap of ZnO-z is estimated by extrapolating the findings for ZnX-z from ZnS-z to ZnO-z. This procedure gave $E_g \approx 3.3$ eV for ZnO-z.

It is well known that not only band gaps are underestimated within LDA and GGA, but also band dispersions come out incorrectly, whereas location of energy levels of the Zn 3d electrons are overestimated (see, e.g., Refs. 20–22 and 63). As also seen from Fig. 2, calculations within the LDA+U approach somewhat correct the location of the energy levels of the Zn 3d electrons. The elucidation of the eigenvalue problem and the order of states at the topmost VB from LDA, GGA, and LDA+U calculations are discussed in Refs. 20–22 and 26 and will not be repeated here.

Examination of Fig. 2 shows that the VB comprises three regions of bands: first a lower region consists of s bands of Zn and X, a higher-lying region of well localized Zn 3d bands, and on top of this a broader band dispersion originating from X-p states hybridized with Zn 3d states. The latter subband is more pronounced in ZnO than in the other ZnX phases considered. The hybridization is most severe according to the LDA and GGA calculations, whereas the LDA+U calculations somehow suppress this and improve the band-gap underestimation. A more detailed discussion of these aspects is found in Refs. 21 and 22.

The SO splitting at the topmost VB is known to play an important role for the electronic structure and chemical bonding of solids.[28,29,32] In semiconductors with z-type structure, the SO splitting energy is determined as the difference between energies of the topmost VB states with symmetry Γ_{8v} and Γ_{7v}.[28,29,32] In the w-type compounds, the topmost VB is split not only by SO interaction but also by CF, giving rise to three states at the Brillouin-zone center. To calculate the SO splitting energy for w-type phases, the quasicubic model of Hopfield[75] is commonly used.

TABLE II. Calculated SO splitting energy (in meV) using the MINDLAB package along with the previous theoretical and experimental findings.

ZnO-z	ZnS-z	ZnSe-z	ZnTe-z
–31	66	432	914
–31	66	432	914
–34[a]	66[a]	393[a]	889[a]
–34[b]	66[b]	398[b]	916[b]
–37[c]	64[c]	392[c]	898[c]
–33[d]	64[d]	393[d]	897[d]
	65[e]	420[f]	910[f]

[a]LAPW, Ref. 28.
[b]LAPW+$p_{1/2}$, Ref. 28.
[c]VASP-PAW, Ref. 28.
[d]VASP-PAW, Ref. 21.
[e]Experiment, Ref. 78.
[f]Experiment, Ref. 79.

It is well known that the SO splitting energy derived from *ab initio* calculations agrees well with experimental data only for some of the semiconductors. This is demonstrated, for example, for all diamondlike group IV and z-type group III-V, II-VI, and I-VII semiconductors,[28] w-type AlN, GaN, and InN,[29] ZnX-w and -z (X=S, Se, and Te),[21,22] and CdTe.[31] However, the errors in estimated SO and CF splitting energies by LDA calculations are significant for semiconductors with strong Coulomb correlation effects, as demonstrated, e.g., for ZnO.[21,22,26] For such systems, DFT calculations within LDA+U (Refs. 21, 22, and 26) are shown to provide quite accurate values for Δ_{CF} and Δ_{SO}. Overestimation of the p-d hybridization in various variants of the DFT can also lead to the wrong spin-orbit coupling of the valence bands.[76,77]

Systematic study of the SO coupling parameters was performed for zinc-blende II-VI semiconductors (Ref. 30) using the TB and LMTO methods, as well as for all diamondlike and zinc-blende semiconductors (Ref. 28) using the FLAPW method with and without the $p_{1/2}$ local orbitals and the frozen-core PAW method implemented into VASP. The corrections coming from the inclusion of the local $p_{1/2}$ orbitals are found to be negligible for the compounds with light atoms. Analysis of these results shows that the SO splitting energy coming from calculations using the VASP-PAW shows good agreement with the experimental data. This result was also obtained[21] recently for ZnX of wurtzite and zinc-blende structures. As demonstrated in Refs. 21 and 22 the SO splitting energy (Δ_{SO}) increases when one moves from ZnO-z to ZnTe-z, in agreement with earlier findings of Ref. 28.

To study the role of the SO coupling in band dispersion, the present *ab initio* calculations have been performed by VASP and MINDLAB packages and spin-orbit splitting energy is found. The results are presented in Table II. Analysis of Table II shows that (Δ_{SO}) calculated by MINDLAB is quite accurate.

As expected, band dispersions calculated with and without the SO coupling differ little when the SO splitting energy

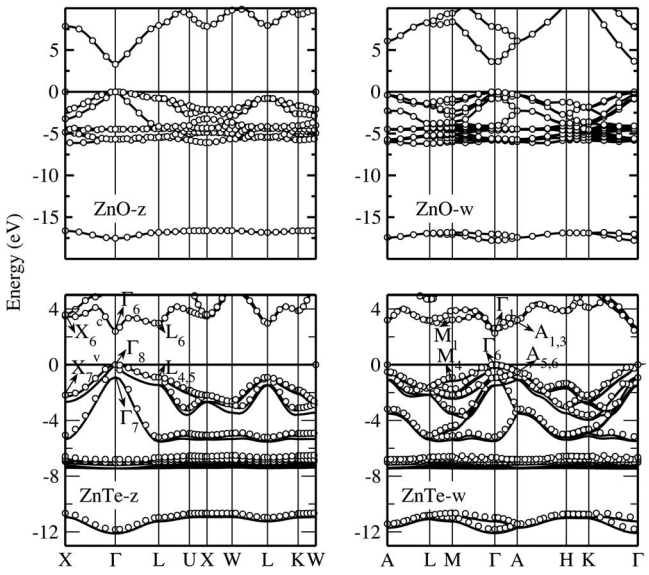

FIG. 4. Band dispersion for ZnO-z, ZnO-w, ZnTe-z, and ZnTe-w calculated by the VASP-PAW method within LDA accounting for SO coupling (solid lines) and without SO coupling (open circles). Topmost VB of the band structure without SO coupling and center of gravity of that with SO coupling are set at zero energy. Symmetry labels for some of the high-symmetry points are shown for (c) ZnTe-z and (d) ZnTe-w to be used for interpretation of the origin of some of the peaks in the optical spectra of ZnX-w and ZnX-z.

is small. However, the difference increases when one moves from ZnO to ZnTe. This feature is demonstrated in Table II and Fig. 4 for band dispersions of ZnO-z, ZnO-w, ZnTe-z, and ZnTe-w calculated by VASP with and without including the SO coupling. As is well known (see, e.g., Refs. 21, 26, and 27), without the SO coupling, the top of the VB of ZnX-w is split into a doublet and a singlet state. In the band structure, the Fermi level is located at the topmost one (Fig. 4), which is the zero energy. Upon inclusion of the SO coupling into calculations, the doublet and singlet states are split into three twofold degenerate states called A, B, and C states with energies $E_g(A)$, $E_g(B)$, and $E_g(C)$, respectively,[80] arranged in order of decreasing energy, i.e., $E_g(A) > E_g(B) > E_g(C)$. The center of gravity of the A, B, and C states, located at $[E_g(A)-E_g(C)]/3$ below the topmost A state, remains to be nearly the same as the topmost VB, corresponding to the case without the SO coupling.[26,27] Consequently, to compare band structures calculated with and without the SO coupling, one should plot the band structure with the Fermi energy at the center of gravity of the A, B, and C states for the former and at the topmost VB for the latter. Hence, when the SO coupling is applied, the A and B states as well as the bottommost CB move upwards to $[E_g(A)-E_g(C)]/3$ in energy, whereas the C state moves downwards to $[E_g(A)-E_g(C)]2/3$ compared to the center of gravity. Then, positions of the lowest VB region calculated with and without the SO coupling remain nearly identical.

B. General features of optical spectra of ZnX

Since optical properties of solids are based on the band structure, the nature of the basic peaks in the optical spectra can be interpreted in terms of the interband transitions responsible for the peaks. Such an interpretation is available for semiconductors with z- and w-type structures.[11,14,81] In order to simplify the presentation of the findings of this work, the labels E_0, E_1, and E_2 of Ref. 11 (from the reflectivity spectra) were retained in Table III and Fig. 4. The subscript 0 is ascribed to transitions occurring at Γ, the subscript 1 to transitions at points in the [111] direction, and the subscript 2 to transitions at points in the [100] direction (referring to the **k** space for the z-type structure). Assignment of the E_0, E_1, and E_2 peaks to optical transitions at high-symmetry points is presented in Table III and Fig. 4.

TABLE III. Relation of the basic E_0, E_1, and E_2 peaks in the optical spectra of ZnX to high-symmetry points (see Refs. 11 and 14) in the Brillouin zone at which the transitions seem to occur.

Peak	z type	w type, $E\|c$	w type, $E\perp c$
E_0	$\Gamma_8\rightarrow\Gamma_6$	$\Gamma_1\rightarrow\Gamma_1$	$\Gamma_6\rightarrow\Gamma_1$
E_1	$L_{4,5}\rightarrow L_6$	$A_{5,6}\rightarrow A_{1,3}$	$M_4\rightarrow M_1$
E_2	$X_7\rightarrow X_6$		

The optical spectra $\epsilon_1(\omega)$, $\epsilon_2(\omega)$, $\alpha(\omega)$, $R(\omega)$, $n(\omega)$, and $k(\omega)$ calculated by DFT within LDA, GGA, and LDA+U are displayed in Figs. 5–8 and compared with available experimental findings.[14] The spectral profiles are indeed very similar to each other. Therefore, we shall only give a brief account mainly focusing on the location of the interband optical transitions. The peak structures in Figs. 5–8 can be explained from the band structure discussed above.

All peaks observed by experiments (see, e.g., Refs. 11 and 14) are reproduced by the theoretical calculations. Because of the underestimation of the optical band gaps in the DFT calculations, the locations of all the peaks in the spectral profiles are consistently shifted toward lower energies as compared with the experimentally determined spectra. Rigid shift (by the scissor operator) of the optical spectra has been applied, which somewhat removed the discrepancy between the theoretical and experimental results. In general, the calculated optical spectra qualitatively agree with the experimental data. In our theoretical calculations, the intensity of the major peaks are underestimated, while the intensity of some of the shoulders is overestimated. This result is in good agreement with previous theoretical findings (see, e.g., Ref. 19). The discrepancies are probably originating from the neglect of the Coulomb interaction between free electrons and holes (excitons), overestimation of the optical matrix elements, and local-field and finite-lifetime effects. Furthermore, for calculations of the imaginary part of the dielectric-response function, only the optical transitions from occupied to unoccupied states with fixed **k** vector are considered. Moreover, the experimental resolution smears out many fine features, and, as demonstrated in Fig. 1, there is inconsistency between the experimental data measured by the same method and at the same temperature. However, as noted in the Introduction, accounting for the excitons and Coulomb correlation effects in *ab initio* calculations[20] by the LAPW+LO within LDA+U allowed correcting not only the energy

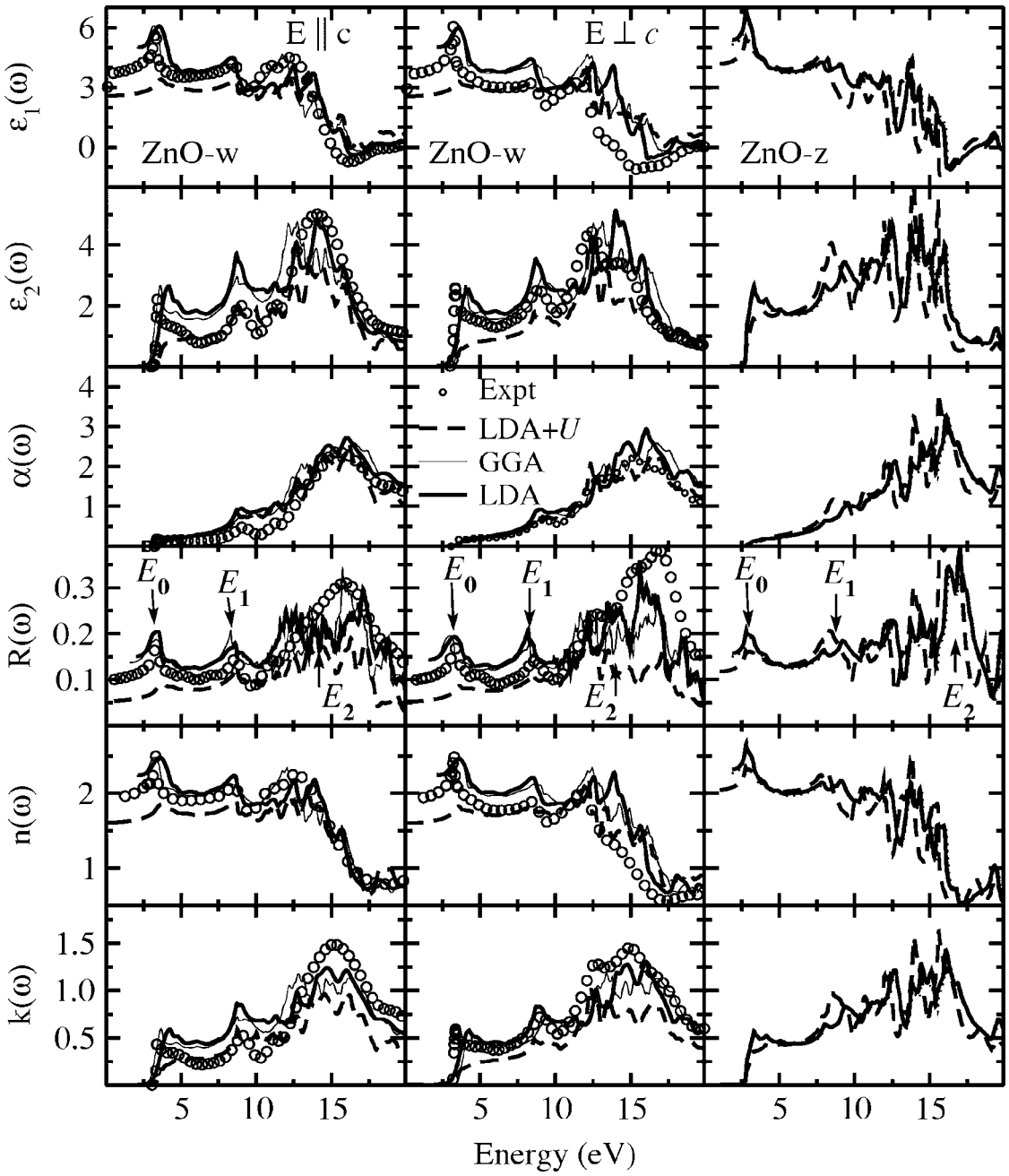

FIG. 5. Optical spectra of ZnO-*w* for $E \| c$ (first column) and $E \perp c$ (second column) and ZnO-*z* (third column). In the first and second columns, the results obtained from calculations are plotted by thick solid lines for LDA, thinner solid lines for GGA, and dashed lines for LDA+*U* and compared with experimental data from Ref. 14 (open circles). In the third column, results calculated within LDA (solid lines), GGA (dotted lines), and LDA+*U* (dashed lines). $\alpha(\omega)$ is given in cm^{-1} divided by 10^5.

position of the Zn 3*d* electrons and eigenvalues but also the optical response. Consequently, accounting for the excitons plays an important role in the optical spectra.

The optical spectra calculated within LDA, GGA, and LDA+*U* do not differ significantly from each other for the Zn*X*-*w* and -*z* phases except for ZnO-*w* and -*z*, for which the optical spectra calculated within LDA+*U* are significantly different from those obtained by LDA and GGA. The difference between the optical spectra calculated by LDA and GGA and those calculated by LDA+*U* decreases when one moves from ZnO to ZnTe. For ZnTe, the difference can be said to be very small. This feature shows that in ZnO-*w* and -*z*, Coulomb correlation effects are strong compared to the other Zn*X*-*w* and -*z* phases, in agreement with recent LAPW+LO calculations[20] including electron-hole correlations.

Comparison of the optical spectra for $E \perp c$ and $E \| c$ for each of the Zn*X*-*w* phases with the isotropic spectra of the corresponding Zn*X*-*z* phases shows that the locations of the peaks almost coincide. This similarity reflects that there is only small differences in the local arrangement of the atoms in the Zn*X*-*w* and corresponding -*z* phases.

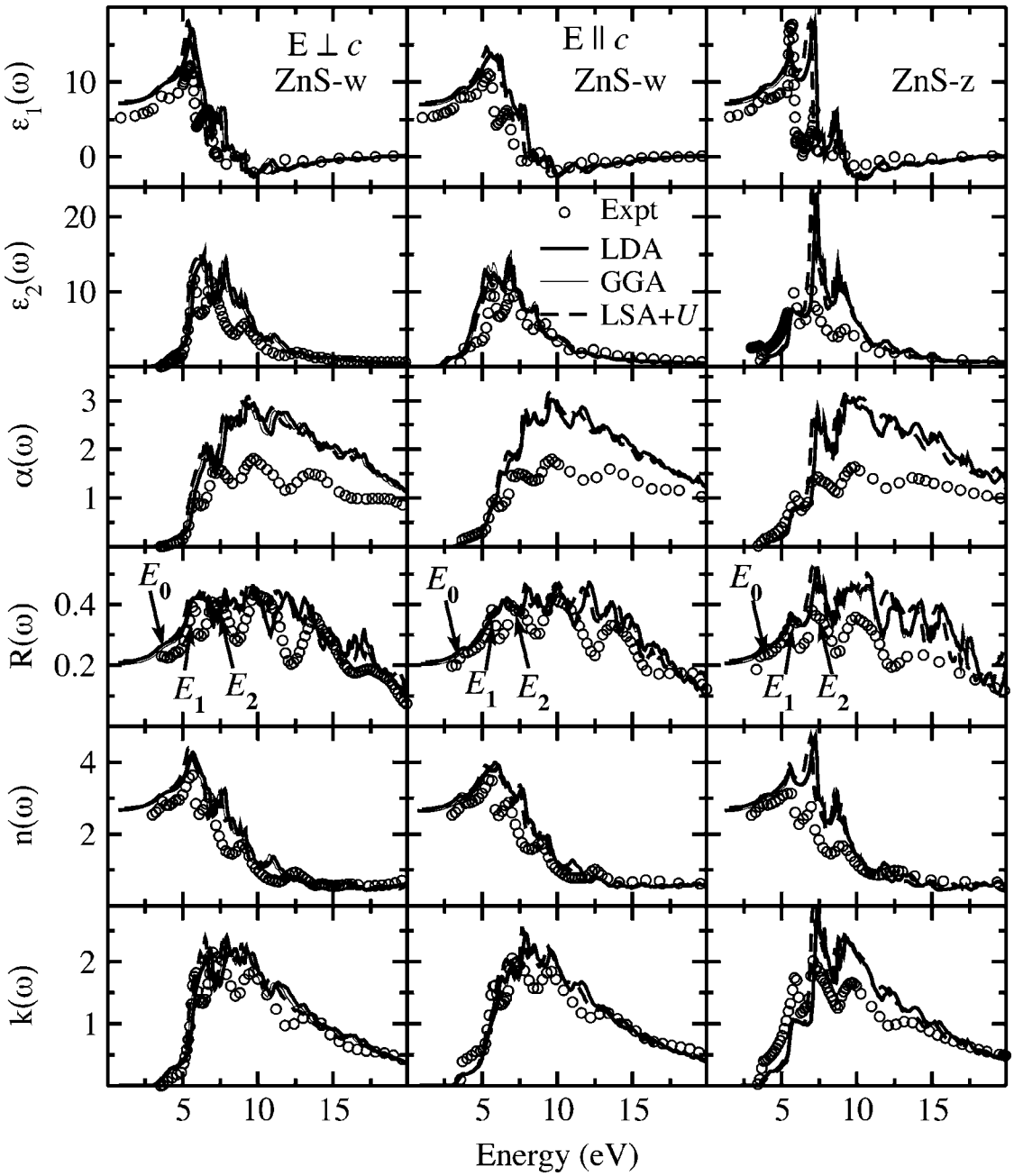

FIG. 6. Optical spectra of ZnS-*w* for $E \| c$ (first column) and $E \perp c$ (second column) and ZnS-*z* (third column) calculated within LDA (thick solid lines), GGA (thin solid lines), and LDA+U (dashed lines) and compared with experimental data (open circles) from Ref. 14. $\alpha(\omega)$ is given in cm^{-1} divided by 10^5.

C. ZnO-*w* and ZnO-*z*

The optical spectra of ZnO-*w* and -*z* calculated by DFT within LDA, GGA, and LDA+U, together with measured data, are displayed in Fig. 5. One clearly sees three major peaks in the experimental spectra located in the energy ranges 3.1–3.3 (E_0), 7.5–8.5 (E_1), and 10–15 eV (E_2). In the E_2 peak, $\epsilon_2(\omega)$, $\alpha(\omega)$, $R(\omega)$, and $k(\omega)$ are seen to take larger values than those in the E_0 and E_1 peaks. This is one of the major features, which distinguishes ZnO-*w* and -*z* from the other Zn*X* phases.

It should be noted that with increasing value of the parameter U in the LDA+U calculations, the intensity of the E_0 and E_1 peaks of ZnO-*w* decreases compared with the LDA and GGA findings as well as with the experimental data. However, the intensity of the E_1 peak of ZnO-*z* from the LDA+U calculations has increased and has become even larger than those derived from the LDA and GGA calculations as well as the experimental data. The intensity of the E_2 peak from the LDA+U calculations oscillates significantly, showing disagreement with the LDA and GGA calculations as well as the experimental measurements. Hence, although LDA+U calculations[21] were good in increasing the LDA-derived band gap and the SO splitting energy as well as in decreasing the crystal-field splitting energy and improving

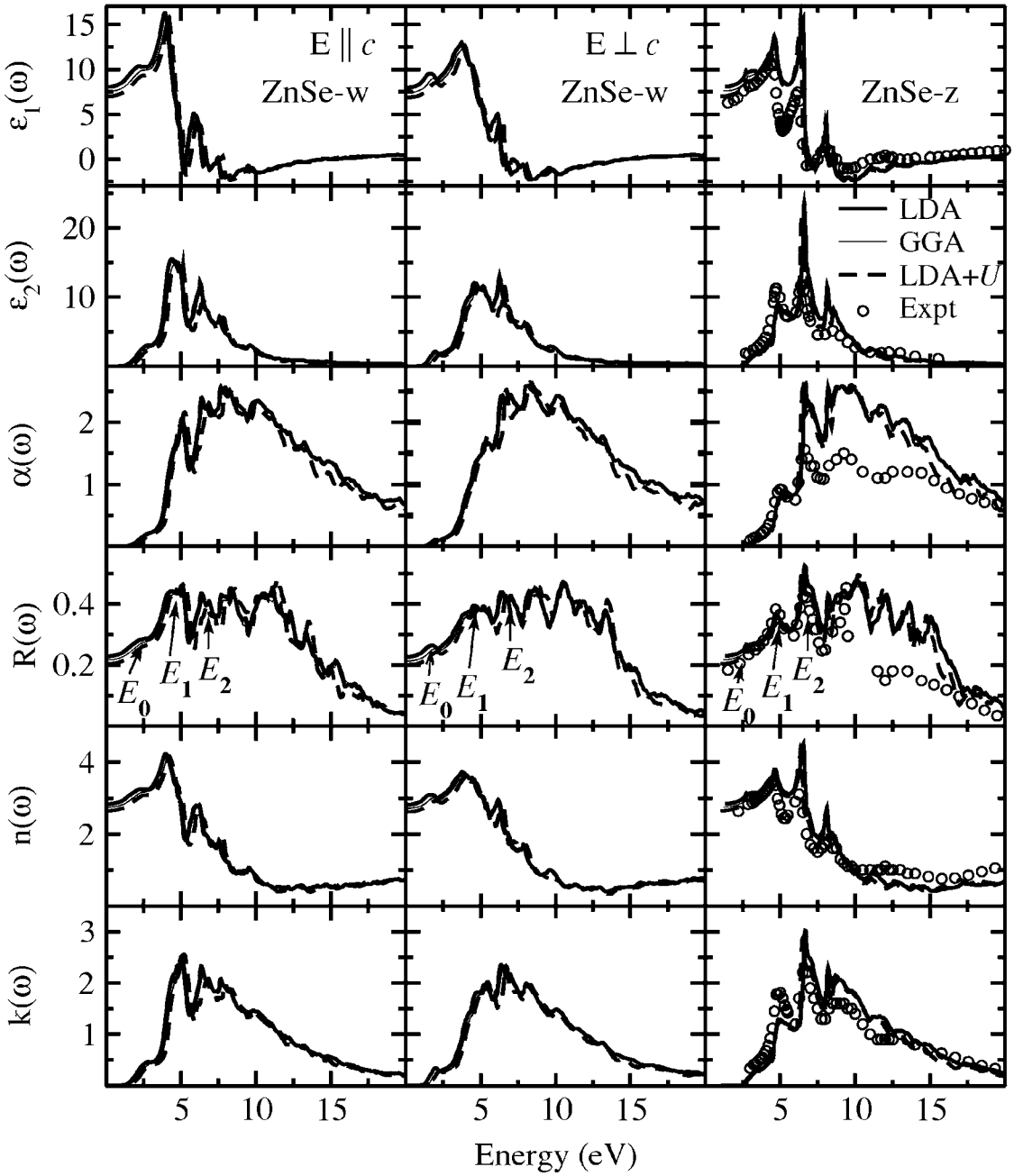

FIG. 7. Optical spectra of ZnSe-w for $E\|c$ (first column) and $E\perp c$ (second column) and ZnSe-z (third column) calculated within LDA (thick solid lines), GGA (thin solid lines), and LDA+U (dashed lines) and compared with experimental data (open circles) from Ref. 14. $\alpha(\omega)$ is given in cm^{-1} divided by 10^5.

the band dispersion, it was poorer than LDA and GGA in describing the optical properties of the ZnO phases. Probably, this discrepancy comes about because in our *ab initio* calculations, electron-hole interactions and SO coupling are not included.[20] The strong variation of the optical properties with increasing values of U indicates appreciable Coulomb correlation effects in ZnO-w and -z, in agreement with our previous band-structure findings[21,22] and LAPW+LO calculations[20] including excitonic effect. This feature is not present in the spectra for the other ZnX-w and -z phases considered.

For convenience of analysis, the $\epsilon_2(\omega)$ profile was analyzed by adjusting the peak location to the experimental data of Ref. 14 by rigid shift. On comparing this result with that of Ref. 8, it is concluded that the peaks at 3.40 eV for $E\|c$ and that at 3.33 eV for $E\perp c$ of $\epsilon_2(\omega)$ and $R(\omega)$ can be ascribed to transitions at the fundamental absorption edge. As shown in Ref. 8, the energy difference (0.07 eV) between these two peaks gives the separation between the so-called A and B (for $E\perp c$) and C (for $E\|c$) states forming the topmost VB of w-type semiconductors, in agreement with 0.083 eV according to the band-structure analyses in Refs. 21 and 22.

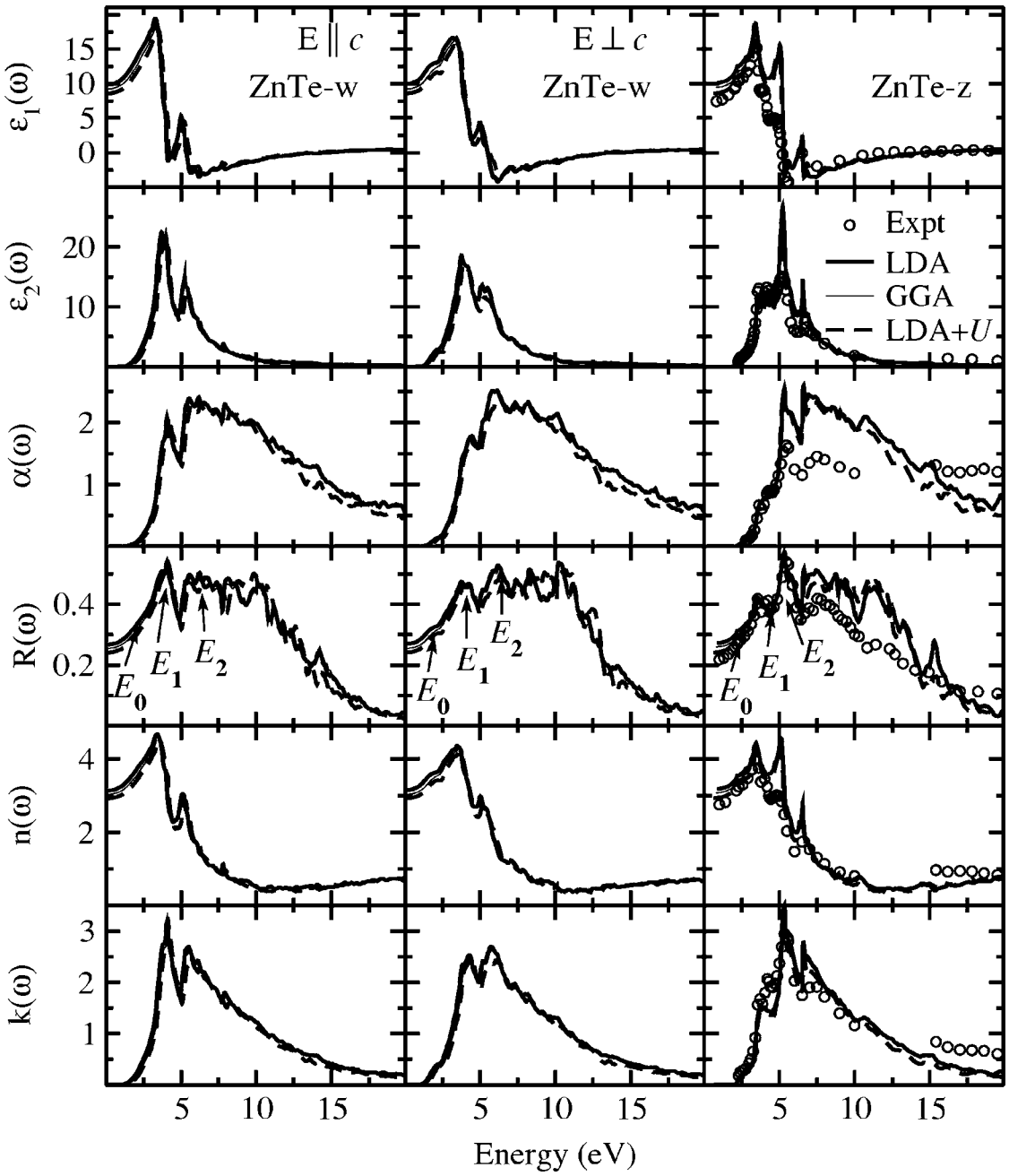

FIG. 8. Optical spectra of ZnTe-*w* for $E\|c$ (first column) and $E\perp c$ (second column) and ZnTe-*z* (third column) calculated within LDA (thick solid lines), GGA (thin solid lines), and LDA+*U* (dashed lines) and compared with experimental data (open circles) from Ref. 14. $\alpha(\omega)$ is given in cm^{-1} divided by 10^5.

There are two broad shoulders of the peak E_0 located at 4.44 and 5.90 eV for $E\perp c$ and 3.90 and 5.29 eV for $E\|c$. Similar shoulders are found at lower energies in the experimental spectra of Refs. 8 and 82 observed at 3.35 and 3.41 eV for $E\perp c$ and 3.39 and 3.45 eV for $E\|c$, and the origin of these shoulders has been ascribed to exciton-phonon coupling. However, in our *ab initio* studies, excitons and lattice vibrations are not taken into consideration.

D. ZnS-*w* and ZnS-*z*

The experimental[14] optical spectra for the ZnS-*w* and -*z* phases are displayed in Fig. 6, together with those calculated according to the LDA, GGA, and LDA+*U*. It is seen that the magnitudes of the experimentally[11] observed shoulders around the E_2 peak in the reflectivity spectra of ZnS-*w* are overestimated in the DFT calculations. As a result, the intensities of the shoulders are almost the same as the intensities of the peaks E_1 and E_2 for $E\perp c$ and even exceeds them for $E\|c$.

The calculated optical spectra for ZnS-*w* by LDA, GGA, and LDA+*U* turned out to be almost identical at energies below 10 eV. However, at higher energies, the LDA- and GGA-derived peaks differ from those obtained by LDA+*U*. This difference can be associated with Zn 3*d* electrons,

which were shifted toward lower energies in the LDA+U calculations. Hence, in ZnS-w and -z, the Coulomb correlation effects appear to play a significant role in optical properties at energies higher than 10 eV.

Compared to ZnO-w, the calculated optical spectra of ZnS-w and -z show larger disagreement with the experimental data. The discrepancy is quite pronounced in the absorption and reflectivity spectra of ZnS-w and -z, especially at energies exceeding 7 eV. The magnitude of the peaks located at higher energies are overestimated significantly compared to the experimental data. The overestimation is more severe in ZnS-z than in ZnS-w as judged from the intensity of the E_2 peak.

E. ZnSe-w, ZnTe-w, ZnSe-z, and ZnSe-z

The optical spectra for ZnSe-w, ZnSe-z, ZnTe-w, and ZnTe-z calculated by DFT within LDA, GGA, and LDA+U are displayed in Figs. 7 and 8, together with the corresponding experimental spectra. Since experimental optical spectra for ZnSe-w and ZnTe-w are not available, rigid shift of the parameters toward higher energies has been performed on the basis of the reflectivity spectra for ZnSe-z and ZnTe-z (Figs. 7 and 8). A closer inspection of Figs. 7 and 8 shows that the optical spectra calculated within LDA, GGA, and LDA+U are almost the same for all selenide and telluride phases. The small differences noted in the absorption and reflectivity spectra appear to originate from the Zn $3d$ electrons.

The location and magnitude of the experimentally measured E_1 peak in the reflectivity spectra of ZnSe-z and ZnTe-z have been assigned[14,11] to fundamental absorption and $\Lambda_3-\Lambda_1$ transitions at the [0.17,0.17,0.17] point of the Brillouin zone. These assignments agree well with theoretical calculations. However, the theoretical calculations did not locate the $E_1+\Delta_1$ peak on the high-energy side of the E_1 peak, which was observed experimentally for both ZnSe-z and ZnTe-z. The reason is certainly that SO coupling was not included in the calculations.

The experimental[13] E_0 peak in the reflectivity spectra, corresponding to transitions at $\mathbf{k}=\mathbf{0}$ [viz., from the highest state of VB (Γ_{15}) to the lowest state of CB (Γ_1)], is well reproduced by the theoretical calculations. One also sees the $E_0+\Delta_0$ peak in the theoretical spectra, which was previously[13] ascribed to SO splitting. Since SO coupling was neglected in the theoretical calculations, the origin of the $E_0+\Delta_0$ peak is not likely to be related to SO coupling.

Similar to the findings for ZnS-z, the theoretically calculated optical spectra for the lower-energy regions of ZnSe-z and ZnTe-z agree with experimental findings. However, the intensity of the peaks located at higher energies is overestimated in the DFT calculations. Anyway, this discrepancy is not as severe as that for ZnS-z. The calculated reflectivity spectra agree well with experimental data in the energy range $\leqslant$6 eV. At higher energies (6–15 eV), LDA, GGA, and LDA+U all overestimate the intensity of the reflectivity. Fairly good agreement with the experimental data is achieved in the energy range 15–20 eV for the real and imaginary parts of the dielectric function for ZnSe-z and ZnTe-z. For the other optical spectra of ZnSe-z and ZnTe-z, the agreement between theory and experiment is poorer.

F. Influence of spin-orbit splitting on the optical spectra of ZnX

It is well known that SO splitting at the top of the VB of a semiconductor is very important for optical transitions, and one should expect large difference in the optical spectra calculated with and without the SO coupling. In this section, we shall analyze how the SO coupling influences the optical spectra of ZnX. For this analysis, *ab initio* band-structure calculations have been performed using the MINDLAB software with and without SO coupling. Based on the band-structure studies, the dielectric-response function $\epsilon_2(\omega)$ has been calculated. The results for ZnX-z are presented in Fig. 9 and compared with experimental data, where it is seen that $\epsilon_2(\omega)$ calculated for ZnO-z without SO coupling is slightly higher than that with the SO coupling, with the main deviations occurring at 3.44–6.00 and 10.00–12.00 eV. The reason for the small distinctions in $\epsilon_2(\omega)$ in this case is the small SO splitting energy.

Our findings show that the SO splitting influences the calculated optical spectra and, in particular, it is most pronounced at energies lower than $\sim$12 eV. At higher energies, the difference between the optical spectra calculated with and without SO coupling is fairly small and agrees reasonably well with the experimental data.[14] This statement applies to all ZnX phases studied. It should be noted that intensities of the peaks calculated with SO coupling are generally lower than those obtained without SO coupling and the latter set agrees better with the experimental data than the former. Furthermore, in the experimental spectra, there are low intensity peaks located at 9.4 eV in ZnS-z, 8.4 eV in ZnS-z, and 7.0 eV in ZnTe-z. However, these peaks are not seen in the calculated spectra with the SO coupling. As noted, this discrepancy can be related to the neglect of many of the above factors such as Coulomb interaction between electrons and holes, local-field effects, and indirect transitions etc.

G. Role of the ground-state structure in the optical spectra of ZnX

In this section, we shall analyze optical spectra of ZnX calculated using the experimentally and theoretically determined lattice parameters. To find the lattice parameters from the *ab initio* calculations, the structural optimization has been performed, which includes the following steps: atoms are relaxed keeping the volume and shape of the lattice. After convergence is reached, the resulting lattice and positional parameters have been used as input to optimize atomic positions, shape, and volume of the unit cell altogether. Then, dependence of the total energy on volume is studied. The minimum of the dependence was accepted as the equilibrium state. Lattice and positional parameters corresponding to the minimum are referred to as the theoretically determined lattice parameters. The thus determined theoretical lattice parameters do not deviate much from the experimental ones. These parameters along with the experimentally determined

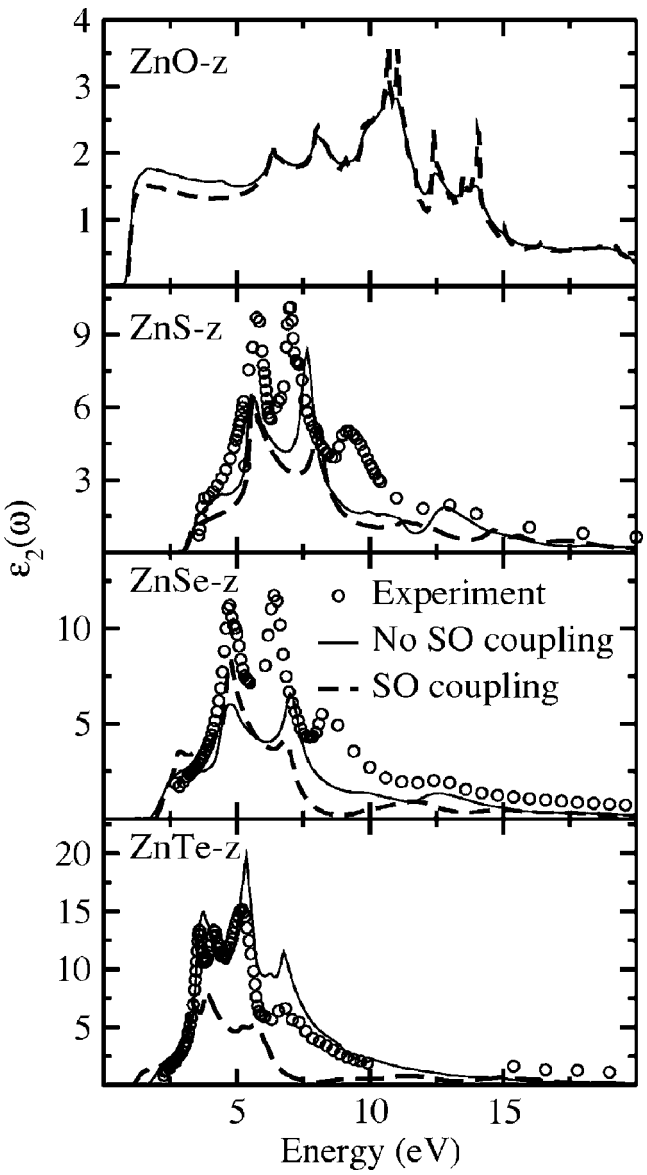

FIG. 9. Imaginary part of the dielectric-response function $\epsilon_2(\omega)$ for ZnO-z, ZnS-z, ZnSe-z, and ZnTe-z calculated by DFT using the MINDLAB package within LDA, including SO coupling into consideration (dashed lines), and without SO coupling (continuous lines), and compared to experimental data (open circles) from Ref. 14.

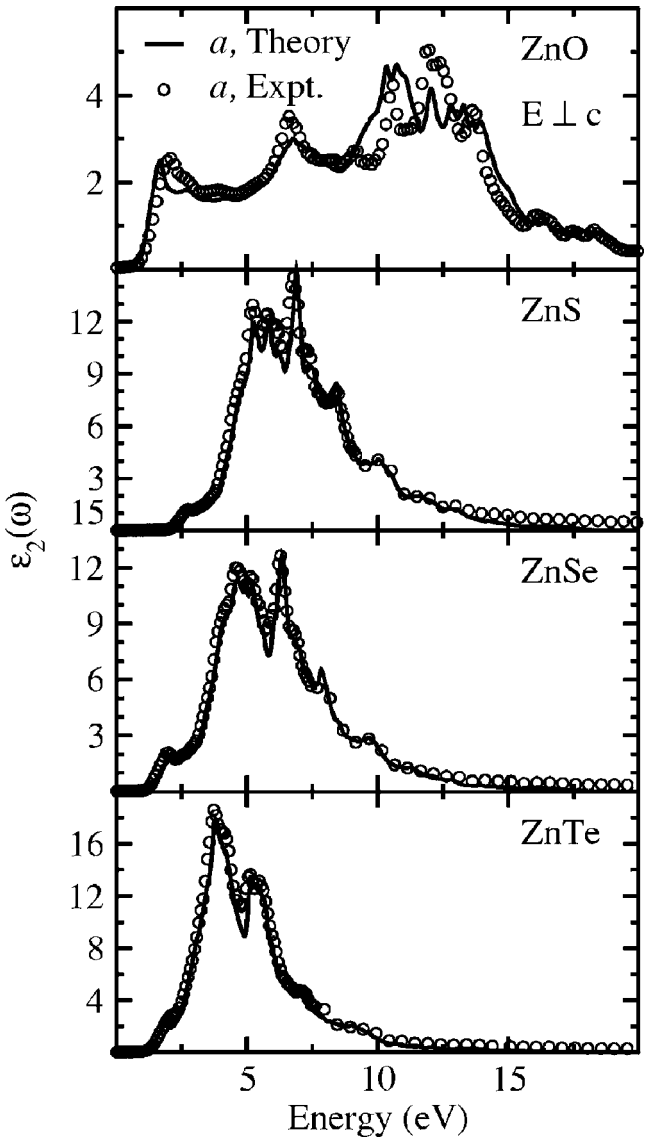

FIG. 10. Imaginary part of the dielectric-response function $\epsilon_2(\omega)$ for ZnX-z calculated by VASP-PAW package using the theoretically (solid lines) and experimentally (open circles) determined lattice parameters.

ones were used for subsequent computations of the electronic structure and optical spectra. The results are presented in Fig. 10 for ZnX-w for $E\perp$. Analysis shows that the optical spectra of ZnO-w for $E\perp$ deviate from each other at energies near the fundamental absorption and at higher energies in the range 8–13 eV. The reason for the difference can be related to changes of the p-d coupling because of the changes of the Zn-O bond lengths coming from structural optimization. Optical spectra of ZnO-w for $E\|c$ and those of other ZnX-w and -z calculated using the theoretical and experimental lattice parameters do not differ from each other significantly.

IV. CONCLUSION

The band structures of the ZnX-w and -z phases (X=O, S, Se, and Te) are calculated by DFT within LDA, GGA, and LDA+U. The topmost VB states are found to be more dispersive than the bottommost CB states. Spin-orbit coupling is found to play an important role for band dispersion, location, and width of the Zn 3d band and the lowest s band. By analyzing the dependence of the band gaps on the atomic number of X for ZnX, the band gap of ZnO-z is estimated to be ~3.3 eV. Using the electronic band structures as references, the optical spectra of ZnX-w and -z are analyzed in the energy range 0–20 eV. The locations of the peaks corresponding to transitions at the fundamental absorption edge calculated by DFT are shifted to lower energies relative to the experimental peaks. This deficiency originates from the well-known errors in band gaps calculated according to DFT. In order to correct the underestimation of band gaps calculated by DFT, the location of the calculated peaks of the optical spectra has been rigidly shifted toward higher energies to match the experimentally determined locations. In the

thus obtained spectra, the locations of the peaks in the lower-energy region agree well with the experimental data. However, the peaks in the higher-energy region agree only tolerably well with the experimental findings. The overall conclusion is that the **k**-independent scissors operator provides a good first approximation for correlation of the underestimated band gaps for the Zn*X*-*w* and -*z* phases. Based on this result, "corrected" band structures of the Zn*X* phases are arranged by adjusting the band gap up to experimentally measured value (viz., rigidly lifting the lowest CB). Not only the locations but also the intensities of some of the calculated low-energy peaks agree with available experimental data for all Zn*X* phases. However, the intensities of some peaks located at higher energies and shoulders have been overestimated. The GGA approach slightly improved the band-gap values. Also, the optical spectra of ZnO-*w* for $E \perp c$ calculated within the GGA agree better with the experimental data than those calculated within the LDA and LDA+U approaches. The value for the corresponding transition at the fundamental absorption edge is decreased and becomes sharper with the use of the GGA, thus providing better agreement with experimental data than LDA. For $E \perp c$, inhomogeneity in the electron gas plays an important role, while it is not so important for $E \| c$. The optical spectra for ZnO-*w* and -*z* calculated within LDA+U for the energy range 0–20 eV are found to depend significantly on the location of the energy levels of the Zn 3*d* electrons. For the other Zn*X*-*w* and -*z* phases, such changes are not so pronounced, in fact, only noticeable at energies above 10 eV. Strong Coulomb correlation effects are established for ZnO-*w* and -*z*. According to the present LDA+U calculations, the probability for the optical transitions at the fundamental absorption edge of ZnO-*w* and -*z* decreases with increasing U. Optical spectra for ZnO-*z*, ZnSe-*w*, and ZnTe-*w* have been predicted. The influence of the spin-orbit coupling is found to increase with increasing the atomic number of the *X* component of Zn*X*.

ACKNOWLEDGMENTS

This work has received financial and supercomputing support from the Research Council of Norway and Academy of Sciences of Uzbekistan (Project No. N31-36,24-06). The authors are thankful to R. Vidya for critical reading of the manuscript and comments. We also thank P. Vajeeston, A. Klaveness, and Dr. K. Knizek for computation-practical help.

[1] H. Yoshikawa and S. Adachi, Jpn. J. Appl. Phys., Part 1 **36**, 6237 (1997).
[2] K. Postava, H. Sueki, M. Aoyama, T. Yamaguchi, C. Ino, Y. Igasaki, and M. Horie, J. Appl. Phys. **87**, 7820 (2000).
[3] K. Postava, H. Sueki, M. Aoyama, T. Yamaguchi, K. Murakami, and Y. Igasaki, Appl. Surf. Sci. **175-176**, 543 (2001).
[4] P. L. Washington, H. C. Ong, J. Y. Dai, and R. Chang, Appl. Phys. Lett. **72**, 3261 (2000).
[5] J. F. Muth, R. M. Kolbas, A. K. Sharma, S. Oktyabrsky, and J. Narayan, J. Appl. Phys. **85**, 7884 (1999).
[6] V. Srikant and D. R. Clarke, J. Appl. Phys. **83**, 5447 (1998).
[7] R. L. Hengehold, R. J. Almassy, and F. L. Pedrotti, Phys. Rev. B **1**, 4784 (1970).
[8] R. Klucker, H. Nelkowski, Y. S. Park, M. Skibowski, and T. S. Wagner, Phys. Status Solidi B **45**, 265 (1971).
[9] J. L. Freeouf, Phys. Rev. B **7**, 3810 (1973).
[10] M. Cardona and R. Haensel, Phys. Rev. B **1**, 2605 (1970).
[11] M. Cardona and G. Harbeke, Phys. Rev. **137**, A1467 (1965).
[12] A. E. Merad, M. B. Kanoun, G. Merad, J. Cibert, and H. Aourag, Mater. Chem. Phys. **92**, 333 (2005).
[13] M. Cardona and D. L. Greenaway, Phys. Rev. **131**, 98 (1963).
[14] *Optical Constants of Crystalline and Amorphous Semiconductors: Numerical Data and Graphical Information*, edited by S. Adachi (Kluwer Academic, Boston, 1999).
[15] V. V. Sobolev and V. V. Sobolev, Phys. Low-Dimens. Semicond. Struct. **9/10**, 113 (2003).
[16] P. Hohenberg and W. Kohn, Phys. Rev. **136**, B864 (1964).
[17] W. Kohn and L. J. Sham, Phys. Rev. **140**, A1133 (1965).
[18] Y.-N. Xu and W. Y. Ching, Phys. Rev. B **48**, 4335 (1993).
[19] C. S. Wang and B. M. Klein, Phys. Rev. B **24**, 3417 (1981).
[20] R. Laskowski and N. E. Christensen, Phys. Rev. B **73**, 045201 (2006).
[21] S. Z. Karazhanov, P. Ravindran, U. Grossner, A. Kjekshus, H. Fjellvåg, and B. G. Svensson, J. Appl. Phys. **100**, 043709 (2006).
[22] S. Z. Karazhanov, P. Ravindran, U. Grossner, A. Kjekshus, H. Fjellvåg, and B. G. Svensson, J. Cryst. Growth **287**, 162 (2006).
[23] V. I. Anisimov, I. V. Solovyev, M. A. Korotin, M. T. Czyzyk, and G. A. Sawatzky, Phys. Rev. B **48**, 16929 (1993).
[24] S. L. Dudarev, G. A. Botton, S. Y. Savrasov, C. J. Humphreys, and A. P. Sutton, Phys. Rev. B **57**, 1505 (1998).
[25] O. Bengone, M. Alouani, P. Blöchl, and J. Hugel, Phys. Rev. B **62**, 16392 (2000).
[26] W. R. L. Lambrecht, A. V. Rodina, S. Limpijumnong, B. Segall, and B. K. Meyer, Phys. Rev. B **65**, 075207 (2002).
[27] L. C. Lew Yan Voon, M. Willatzen, M. Cardona, and N. E. Christensen, Phys. Rev. B **53**, 10703 (1996).
[28] P. Carrier and S.-H. Wei, Phys. Rev. B **70**, 035212 (2004).
[29] S.-H. Wei and A. Zunger, Appl. Phys. Lett. **69**, 2719 (1996).
[30] M. Willatzen, M. Cardona, and N. E. Christensen, Phys. Rev. B **51**, 17992 (1995).
[31] S. Lalitha, S. Z. Karazhanov, P. Ravindran, S. Senthilarasu, R. Sathyamoorthy, and J. Janabergenov, Physica B **387**, 227 (2006).
[32] R. F. W. Bader, *Atoms in Molecules: A Quantum Theory* (Oxford University Press, New York, 1990).
[33] M. Cardona, N. E. Christensen, and G. Fasol, Phys. Rev. B **38**, 1806 (1995).
[34] M. Usuda, N. Hamada, T. Kotani, and M. van Schilfgaarde, Phys. Rev. B **66**, 125101 (2002).
[35] M. Oshikiri and F. Aryasetiawan, J. Phys. Soc. Jpn. **69**, 2113 (2000).
[36] A. Fleszar and W. Hanke, Phys. Rev. B **71**, 045207 (2005).
[37] P. Rinke, A. Qteish, J. Neugebauer, C. Freysoldt, and M. Schef-

fler, New J. Phys. **7**, 126 (2005).
[38] M. Städele, M. Moukara, J. A. Majewski, P. Vogl, and A. Görling, Phys. Rev. B **59**, 10031 (1999).
[39] S. Sharma, J. K. Dewhurst, and C. Ambrosch-Draxl, Phys. Rev. Lett. **95**, 136402 (2005).
[40] R. Asahi, W. Mannstadt, and A. J. Freeman, Phys. Rev. B **59**, 7486 (1999).
[41] L. X. Benedict, E. L. Shirley, and R. B. Bohn, Phys. Rev. B **57**, R9385 (1998).
[42] F. Bechstedt, K. Tenelsen, B. Adolph, and R. Del Sole, Phys. Rev. Lett. **78**, 1528 (1997).
[43] G. A. Baraff and M. Schlüter, Phys. Rev. B **30**, 3460 (1984).
[44] A. Delin, P. Ravindran, O. Eriksson, and J. M. Wills, Int. J. Quantum Chem. **69**, 349 (1998).
[45] P. Ravindran, A. Delin, B. Johansson, O. Eriksson, and J. M. Wills, Phys. Rev. B **59**, 1776 (1999).
[46] *Inorganic Crystal Structure Database* (Gmelin Institut, Karlsruhe, 2001).
[47] *Handbook of Laser Science and Technology*, edited by M. J. Weber (CRC, Cleveland, 1986), Vol. III.
[48] O. Zakharov, A. Rubio, X. Blase, M. L. Cohen, and S. G. Louie, Phys. Rev. B **50**, 10780 (1994).
[49] N. Lakshmi, N. M. Rao, R. Venugopal, D. R. Reddy, and B. K. Reddy, Mater. Chem. Phys. **82**, 764 (2003).
[50] V. N. Tomashik, G. S. Oleinik, and I. B. Mizetskaya, Inorg. Mater. **14**, 1119 (1978).
[51] W. H. Bragg and J. A. Darbyshire, J. Met. **6**, 238 (1954).
[52] *Semiconductors: Physics of Group IV Elements and III-V Compounds*, edited by K.-H. Hellwege and O. Madelung, Landolt-Boörnstein, New series, Group III, Vol. 17, Pt. A (Springer-Verlag, Berlin, 1982); *Theoretical Structures of Molecules*, edited by P. von Ragué Schleyer, Landolt-Börnstein, New Series, Group II, Vol. 22, Pt. A (Springer-Verlag, Berlin, 1993).
[53] *CRC Handbook of Chemistry and Physics*, 70th ed., edited by R. C. Weast, D. R. Lide, M. J. Astle, and W. H. Beyer (CRC, Boca Raton, FL,1990).
[54] B. K. Agrawal, P. S. Yadav, and S. Agrawal, Phys. Rev. B **50**, 14881 (1994).
[55] G. Kresse and J. Furthmüller, Phys. Rev. B **54**, 11169 (1996).
[56] J. P. Perdew, K. Burke, and M. Ernzerhof, Phys. Rev. Lett. **77**, 3865 (1996).
[57] J. P. Perdew and A. Zunger, Phys. Rev. B **23**, 5048 (1981).
[58] D. M. Ceperley and B. J. Alder, Phys. Rev. Lett. **45**, 566 (1980).
[59] P. E. Blöchl, Phys. Rev. B **50**, 17953 (1994).
[60] G. Kresse and D. Joubert, Phys. Rev. B **59**, 1758 (1999).
[61] B. Adolph, J. Furthmüller, and F. Bechstedt, Phys. Rev. B **63**, 125108 (2001).
[62] D. Vogel, P. Krüger, and J. Pollmann, Phys. Rev. B **52**, R14316 (1995).
[63] C. L. Dong, C. Persson, L. Vayssieres, A. Augustsson, T. Schmitt, M. Mattesini, R. Ahuja, C. L. Chang, and J.-H. Guo, Phys. Rev. B **70**, 195325 (2004).
[64] A. Janotti and C. G. Van de Walle, J. Cryst. Growth **287**, 58 (2006).
[65] W. E. Pickett, S. C. Erwin, and E. C. Ethridge, Phys. Rev. B **58**, 1201 (1998).
[66] M. Ruckh, D. Schmid, and H. W. Schock, J. Appl. Phys. **76**, 5945 (1994).
[67] S. Y. Savrasov, Phys. Rev. B **54**, 16470 (1996).
[68] O. Gunnarsson and B. I. Lundqvist, Phys. Rev. B **13**, 4274 (1976).
[69] S. H. Vosko, L. Wilk, and M. Nusair, Can. J. Phys. **58**, 1200 (1980).
[70] P. Ravindran, A. Delin, R. Ahuja, B. Johansson, S. Auluck, J. M. Wills, and O. Eriksson, Phys. Rev. B **56**, 6851 (1997).
[71] P. Ravindran, A. Delin, P. James, B. Johansson, J. M. Wills, R. Ahuja, and O. Eriksson, Phys. Rev. B **59**, 15680 (1999).
[72] D. Vogel, P. Krüger, and J. Pollmann, Phys. Rev. B **54**, 5495 (1996).
[73] *Semiconductors: Other than Group IV Elements and IV Elements and III-V Compounds*, edited by O. Madelung (Springer, Berlin, 1992).
[74] K. Hümmer, Phys. Status Solidi B, **56**, 249 (1973).
[75] J. J. Hopfield, J. Phys. Chem. Solids **15**, 97 (1960).
[76] S.-H. Wei and A. Zunger, Phys. Rev. B **39**, 3279 (1989).
[77] S.-H. Wei and A. Zunger, Phys. Rev. B **37**, 8958 (1988).
[78] *Semiconductors: Physics of Group IV Elements and III-V Compounds*, edited by O. Madelung, M. Schulz, and H. Weiss, Landolt-Bömstein, New Series, Group III, Vol. 17, Pt. A (Springer, Berlin, 1982).
[79] *Semiconductors: Basic Data*, 2nd ed., edited by O. Madelung (Springer, Berlin, 1996).
[80] A. Mang, K. Reimann, and S. Rübenacke, Solid State Commun. **94**, 251 (1995).
[81] M. L. Cohen and J. R. Chelikowsky, *Electronic Structure and Optical Properties of Semiconductors* (Springer, Berlin, 1988).
[82] W. Y. Liang and A. D. Yoffe, Phys. Rev. Lett. **20**, 59 (1968).